Photoelectron spectroscopy of boron-gold alloy clusters and boron boronyl clusters: B3Au n and B3(BO) n (n = 1, 2)

Qiang Chen, Hui Bai, Hua-Jin Zhai, Si-Dian Li, and Lai-Sheng Wang

Citation: The Journal of Chemical Physics **139**, 044308 (2013); doi: 10.1063/1.4816010
View online: http://dx.doi.org/10.1063/1.4816010
View Table of Contents: http://scitation.aip.org/content/aip/journal/jcp/139/4?ver=pdfcov
Published by the AIP Publishing

Articles you may be interested in

Pi and sigma double conjugations in boronyl polyboroene nanoribbons: B n (BO)2 and B n (BO)2 (n = 512)
J. Chem. Phys. **139**, 174301 (2013); 10.1063/1.4827501

On the structures and bonding in boron-gold alloy clusters: B6Au n and B6Au n (n = 13)
J. Chem. Phys. **138**, 084306 (2013); 10.1063/1.4792501

Experimental and theoretical studies on the electronic properties of vanadium-benzene sandwich cluster anions, V n Bz n+1 (n = 1-5)
J. Chem. Phys. **137**, 224305 (2012); 10.1063/1.4769776

Vibrationally resolved photoelectron imaging of platinum carbonyl anion Pt(CO) n (n = 1-3): Experiment and theory
J. Chem. Phys. **137**, 204302 (2012); 10.1063/1.4768004

Probing the structures and chemical bonding of boron-boronyl clusters using photoelectron spectroscopy and computational chemistry: B4(BO) n (n = 1–3)
J. Chem. Phys. **137**, 044307 (2012); 10.1063/1.4737863

This article is copyrighted as indicated in the article. Reuse of AIP content is subject to the terms at: http://scitation.aip.org/termsconditions. Downloaded to IP: 128.148.231.12 On: Mon, 26 May 2014 19:58:53

Photoelectron spectroscopy of boron-gold alloy clusters and boron boronyl clusters: $B_3Au_n^-$ and $B_3(BO)_n^-$ ($n = 1, 2$)

Qiang Chen,[1] Hui Bai,[1] Hua-Jin Zhai,[1,2,a)] Si-Dian Li,[1,a)] and Lai-Sheng Wang[2,b)]
[1]*Institute of Molecular Science, Shanxi University, Taiyuan 030006, People's Republic of China*
[2]*Department of Chemistry, Brown University, Providence, Rhode Island 02912, USA*

(Received 28 May 2013; accepted 4 July 2013; published online 25 July 2013)

Photoelectron spectroscopy and density-functional theory are combined to study the structures and chemical bonding in boron-gold alloy clusters and boron boronyl clusters: $B_3Au_n^-$ and $B_3(BO)_n^-$ ($n = 1, 2$). Vibrationally resolved photoelectron spectra are obtained for all four species and the B−Au and B−BO clusters exhibit similar spectral patterns, with the latter species having higher electron binding energies. The electron affinities of B_3Au, B_3Au_2, $B_3(BO)$, and $B_3(BO)_2$ are determined to be 2.29 ± 0.02, 3.17 ± 0.03, 2.71 ± 0.02, and 4.44 ± 0.02 eV, respectively. The anion and neutral clusters turn out to be isostructural and isovalent to the $B_3H_n^-/B_3H_n$ ($n = 1, 2$) species, which are similar in bonding owing to the fact that Au, BO, and H are monovalent σ ligands. All $B_3Au_n^-$ and $B_3(BO)_n^-$ ($n = 1, 2$) clusters are aromatic with 2π electrons. The current results provide new examples for the Au/H and BO/H isolobal analogy and enrich the chemistry of boronyl and gold. © *2013 AIP Publishing LLC*. [http://dx.doi.org/10.1063/1.4816010]

I. INTRODUCTION

Due to its intrinsic electron deficiency, boron possesses unique chemical bonding properties, featuring three-center two-electron (3c–2e) bonds in boranes[1] and aromaticity in synthetic boron compounds.[2] Similarly, the bonding in elementary boron clusters is recently shown to be dominated by aromaticity and antiaromaticity as well,[3–12] which lead to planar or quasi-planar cluster structures up to large sizes that are unparalleled in any other element in the periodic table. The concepts of aromaticity and antiaromaticity are applicable for both the π and σ frameworks in the boron clusters. Therefore, species with double aromaticity, double antiaromaticity, or conflicting aromaticity have been observed.[3] Boron alloy clusters and ligated boron complexes offer further opportunities to tune the electronic and bonding properties of elemental boron clusters.[13–20]

The boron trimer anion, B_3^- (D_{3h}, $^1A_1'$), is the simplest species with double (π and σ) aromaticity,[6] which possesses 2π and 2σ delocalized electrons and obeys the $(4n + 2)$ Hückel rule. Neutral B_3 (D_{3h}, $^2A_1'$) cluster is also π aromatic, but it only has one delocalized σ electron, that is, a three-center one-electron (3c–1e) bond. Interestingly, fully hydrogenating B_3^- leads to the C_{2v} $B_3H_8^-$ borane, which has been shown to be a 2-electron σ aromatic system.[21,22] The ammonia derivative of this borane, $NH_3B_3H_7$, was recently synthesized via iodine oxidation and was considered as a potential hydrogen storage material.[23] Ligated boron trimer clusters are interesting molecular models to elucidate how the ligands successively change the structures and aromaticity of boron clusters, and how the delocalized multicenter bonds are transformed to localized two-center two-electron (2c–2e) bonds. The structures of B_3H and B_3H_2 were studied computationally previously,[24] in which the H atoms were shown to prefer terminal positions of the B_3 triangle. Isovalent Al_3H and Al_3H_2 clusters were computed subsequently and similar structures were found.[25,26] However, the isovalent B_3Li was shown to be a charge transfer complex and possess C_{3v} symmetry with the Li atom sitting above the B_3 unit.[27] The B_3H cluster was recently studied at the multireference configuration interaction (MRCI) and coupled-cluster with single, double, and perturbative triple excitations (CCSD(T)) levels.[28] Furthermore, a relevant boronyl $B_3(BO)_3$ complex and its anion and dianion were computationally studied.[29] These clusters are isostructural to the B_3H_3 species owing to the recent discovery of boronyl (BO) as a robust monovalent σ ligand[30] and the BO/H isolobal analogy.[31–41] However, there has been little experimental information available for the ligated B_3 compounds. For higher coordinated complexes, C_{3v} $B_3H_6^+$ was computed to be a 2π aromatic species,[42] a boron analog of cyclopropenium cation. An extensive series of neutral and charged B_3H_n ($n = 3$–9) clusters were also computed, with an emphasis on their aromatic properties.[43] Global minimum searches were performed for B_3H_n ($n = 4$–7) clusters and their anions, which all maintain the B_3 motif.[44]

Here we report a combined photoelectron spectroscopy (PES) and density-functional theory (DFT) study on two boron-gold alloy clusters B_3Au^- and $B_3Au_2^-$ and their corresponding BO clusters, $B_3(BO)^-$ (that is, B_4O^-) and $B_3(BO)_2^-$ (that is, $B_5O_2^-$). A gold atom has been found lately to be isolobal to a H atom when bonding to the Si and B clusters.[13,45–48] Thus, the current B–Au and B–(BO) clusters are expected to display structures similar to the B_3H^- and $B_3H_2^-$ species. We found that these B–Au and B–(BO) clusters show similar experimental PES patterns. Using the combined experimental and computational data, we confirmed that the $B_3Au_n^-$ and $B_3(BO)_n^-$ ($n = 1, 2$) clusters and their

a)Electronic addresses: hj.zhai@sxu.edu.cn and lisidian@sxu.edu.cn.
b)Electronic mail: lai-sheng_wang@brown.edu.

 © 2013 AIP Publishing LLC

This article is copyrighted as indicated in the article. Reuse of AIP content is subject to the terms at: http://scitation.aip.org/termsconditions. Downloaded to IP: 128.148.231.12 On: Mon, 26 May 2014 19:58:53

neutrals are indeed isostructural and isovalent to the corresponding $B_3H_n^-/B_3H_n$ ($n = 1, 2$) species. This study provides new examples for the isolobal analogy of Au, BO, and H, which are all monovalent σ radical ligands.

II. EXPERIMENTAL AND THEORETICAL METHODS

A. Photoelectron spectroscopy

The experiments were carried out using a magnetic-bottle-type PES apparatus equipped with a laser vaporization cluster source, details of which were published in Ref. 49. Briefly, the B_3Au^- and $B_3Au_2^-$ clusters were produced by laser vaporization of an Au/B mixed target (^{10}B enriched) in the presence of a pure helium carrier gas, whereas the B_4O^- and $B_5O_2^-$ clusters were produced using a ^{10}B-enriched disk target in the presence of a helium carrier gas seeded with 0.01% O_2. The cluster anions were analyzed using a time-of-flight mass spectrometer and the cluster species of interest were each mass-selected and decelerated before being photodetached. Photodetachment experiments were conducted at three photon energies: 355 nm (3.496 eV) and 266 nm (4.661 eV) from a Nd:YAG laser and 193 nm (6.424 eV) from an ArF excimer laser. Effort was made to choose colder clusters (that is, those with long resident times in the nozzle) for photodetachment, which was shown previously to be critical for obtaining high quality PES data.[50] Photoelectrons were collected at nearly 100% efficiency by the magnetic bottle and analyzed in a 3.5 m long electron flight tube. The PES spectra were calibrated using the known spectra of Rh^- and Au^-, and the energy resolution of the apparatus was $\Delta E_k/E_k \approx 2.5\%$, that is, ~25 meV for 1 eV kinetic energy electrons.

B. Computational methods

The DFT structural searches for the anion clusters were performed using the Coalescence Kick (CK) global minimum search program,[10,51] initially at the B3LYP/Lanl2dz and B3LYP/3-21G levels for B−Au and B–O systems, respectively.[52,53] The top low-lying candidate structures were then fully optimized at the B3LYP/B,O/aug-cc-pVTZ/Au/Stuttgart_rsc_1997_ecp+2f1g level,[54] which the term "B3LYP" stands for throughout the text, unless stated specifically otherwise. Frequency calculations were done to confirm that the reported structures are true minima unless otherwise stated. Excitation energies of the neutral clusters were calculated using the generalized Koopmans' theorem (GKT)[55] and time-dependent B3LYP (TD-B3LYP) methods[56] at the anion ground-state geometries. Single-point CCSD(T) calculations[57] were done at the B3LYP geometries to further evaluate the relative energies of the low-lying structures and to refine the adiabatic (ADE) and vertical (VDE) detachment energies. All calculations were done using the GAUSSIAN 09 package.[58]

III. EXPERIMENTAL RESULTS

A. B_3Au^-

The PES spectra of B_3Au^- at three photon energies are shown in Fig. 1. The 355 nm spectrum (Fig. 1(a)) reveals a sharp ground-state band X with a short vibrational progression and a frequency of 1040 ± 50 cm^{-1}. The 0–0 transition at 2.29 ± 0.02 eV (Table I) represents the ground-state ADE and VDE, which is also the EA of the neutral cluster. Following a ~1 eV energy gap, band A (VDE: 3.28 eV) is well-resolved at 266 nm (Fig. 1(b)) with a more extensive vibrational progression and a frequency of 1170 cm^{-1}. Band B at a VDE of 3.70 eV is also vibrationally resolved at 266 nm with an estimated vibrational spacing of 1200 cm^{-1}. A pair of bands, C (VDE: 3.94 eV) and D (VDE: 4.34 eV), are broader with no vibrational features, where band C is intense and band D is much weaker. At 193 nm (Fig. 1(c)), a number of bands are observed at the high binding energy side: E, F, G, and H at the VDEs of 4.57, 5.34, 5.60, and ~6.1 eV, respectively.

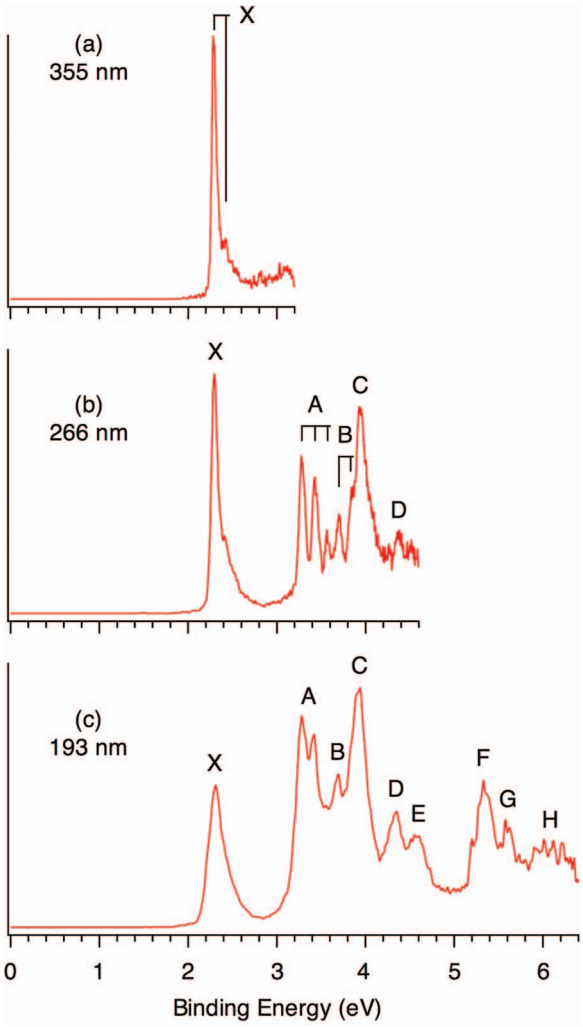

FIG. 1. Photoelectron spectra of B_3Au^- at (a) 355 nm (3.496 eV), (b) 266 nm (4.661 eV), and (c) 193 nm (6.424 eV). The vertical lines represent resolved vibrational structures.

B. $B_3Au_2^-$

The 266 nm PES spectrum of $B_3Au_2^-$ exhibits three broad bands: X, A, and B at VDEs of 3.22, 3.80, and ~4.2 eV, respectively (Fig. 2(a)). Band X is partially vibrationally resolved with an estimated vibrational spacing of ~1150 cm^{-1}. The first vibrational peak of band X is still quite broad,

This article is copyrighted as indicated in the article. Reuse of AIP content is subject to the terms at: http://scitation.aip.org/termsconditions. Downloaded to IP: 128.148.231.12 On: Mon, 26 May 2014 19:58:53

TABLE I. Experimental adiabatic and vertical detachment energies (ADEs and VDEs; in eV) from the photoelectron spectra of B_3Au^- and $B_3Au_2^-$ clusters, as compared with those calculated using the generalized Koopmans' theorem and the time-dependent B3LYP (TD-B3LYP) methods.

	Expt.		Theor. (GKT)		Theor. (TD-B3LYP)	
Species	Feature	*ADE*/VDE[a,b]	MO[c]	*ADE*/VDE[b,c]	Final state	*ADE*/VDE[b]
B_3Au^-	X	*2.29* (*2*)/2.29 (2)[d]	a_1 (α)	*2.45*/2.47 (S)[e]	$^1A_1$	*2.45*/2.47
	A	3.28 (2)	b_1 (β)	3.31 (T)	$^3B_1$	3.12
	B	3.70 (2)	b_1 (α)	3.42 (S)	$^3A_1$	3.48
	C	3.94 (3)	a_1 (β)	3.87 (T)	$^3B_2$	3.68
	D	4.34 (3)	a_1 (α)	4.10 (S)	$^1B_1$	3.79
	E	4.57 (3)	b_2 (β)	4.43 (T)	$^1A_1$	4.58
	F	5.34 (3)	b_2 (α)	5.13 (S)	$^3A_1$	5.11
			a_1 (β)	5.18 (T)	$^1A_1$	5.75
	G	5.60 (3)	a_1 (α)	5.26 (S)	$^1B_2$	5.78
	H	~6.1	a_1 (β)	5.85 (T)	$^3A_2$	6.02
			a_2 (β)	5.85 (T)	$^3A_1$	6.02
			a_2 (α)	5.86 (S)	$^1A_2$	6.15
			a_1 (α)	5.86 (S)	$^1A_1$	6.15
$B_3Au_2^-$	X	*3.17* (*3*)/3.22 (3)[d]	b_1 (α)	*3.04*/3.21 (D)[e]	$^2B_1$	*3.04*/3.21
	A	3.80 (3)	b_2 (α)	3.56 (D)	$^2A_2$	3.54
	B	~4.2	a_1 (α)	3.80 (D)	$^2B_1$	3.79
	C	4.89 (2)	a_1 (α)	5.05 (D)	$^2B_1$	5.09
	D	5.42 (2)	b_2 (α)	5.31 (D)	$^2A_2$	5.38
	E	5.70 (2)	b_2 (α)	5.94 (D)	$^2A_2$	6.05
			a_2 (α)	5.94 (D)	$^2B_2$	6.05
	F	6.15 (5)	b_1 (α)	5.96 (D)	$^2A_1$	6.07
			a_1 (α)	5.96 (D)	$^2B_1$	6.07

[a]Numbers in the parentheses represent experimental uncertainties in the last digit.
[b]Shown in *italic* is the ground-state ADE, that is, the electron affinity of the neutral cluster.
[c]Molecular orbital from which the electron is detached. Labels "α'' and "β'' denote majority and minority spins, respectively; whereas labels "S," "D," and "T" denote singlet, doublet, and triplet final states, respectively.
[d]Observed symmetric vibrational frequencies for B_3Au neutral cluster are 1040 ± 50, 1170 ± 30, 1200 ± 50 cm^{-1} for bands X, A, and B, respectively; whereas those observed for B_3Au_2 neutral cluster are ~1150, ~900, ~950 cm^{-1} for bands X, D, and E, respectively.
[e]Calculated ground-state *ADE*/VDE at CCSD(T)//B3LYP/B/aug-cc-pVTZ/Au/Stuttgart_rsc_ 1997_ecp+2f1g level are *2.03*/2.09 for B_3Au^- and *2.97*/3.25 for $B_3Au_2^-$.

suggesting that it may contain unresolved low frequency vibrations. Thus, the ground-state ADE is estimated by drawing a straight line along the leading edge of the first peak of the X band and then adding the instrumental resolution to the intersection with the binding energy axis. The ADE thus evaluated is 3.17 ± 0.03 eV, which is the EA of neutral B_3Au_2. At 193 nm (Fig. 2(b)), four more bands are resolved: C, D, E, and F at the VDEs of 4.89, 5.42, 5.70, and 6.15 eV, respectively. Band C, D, and E are sharp, whereas band F is relatively broad. Vibrational structures are observed for bands D and E, with vibrational frequencies of ~900 and ~950 cm^{-1}, respectively.

C. B_4O^-

The 355 nm spectrum of B_4O^- (Fig. 3(a)) reveals the ground state band X with well-resloved vibrational structures. The 0–0 transition at 2.71 ± 0.02 eV defines the first ADE, as well as the first VDE, which is also the EA of B_4O. The resolved vibrational structures indicate that two vibrational modes are activated for the neutral ground state with frequencies of 1020 ± 50 cm^{-1} and 730 ± 50 cm^{-1}, whose combination generates the vibrational peak at 2.93 eV. At 266 nm (Fig. 3(b)), three more bands are observed: A, B, and C at VDEs of 3.88, 4.03, and 4.43 eV, respectively. Band A is intense and relatively sharp, band B is weak, and band C is very broad. The high binding energy portion of the 193 nm spectrum (Fig. 3(c)) shows weak electron signals with poor statistics. Three bands are tentatively labeled: D, E, and F at 4.85, ~5.2, and 5.80 eV.

D. $B_5O_2^-$

The 266 nm spectrum of $B_5O_2^-$ shows a well-resolved vibrational progression for the ground-state band X with a frequency of 370 ± 30 cm^{-1} (Fig. 4(a)). A higher frequency mode (1280 ± 50 cm^{-1}) is also revealed at 193 nm (Fig. 4(b)). The 0–0 transition at 4.44 ± 0.02 eV represents the ground-state ADE and VDE, which is also the EA of B_5O_2. Two broad excited-state bands are also observed at 193 nm: A (VDE: 4.90 eV) and B (~5.2 eV).

IV. THEORETICAL RESULTS

The optimized global-minimum structures of B_3Au^-, $B_3Au_2^-$, B_4O^-, and $B_5O_2^-$ and their corresponding neutral clusters are depicted in Fig. 5. Alternative low-lying anion structures are summarized in Figs. S1–S4 in the supplementary material,[59] along with their relative energies. Zero-point energy (ZPE) corrections were not considered,

This article is copyrighted as indicated in the article. Reuse of AIP content is subject to the terms at: http://scitation.aip.org/termsconditions. Downloaded to IP: 128.148.231.12 On: Mon, 26 May 2014 19:58:53

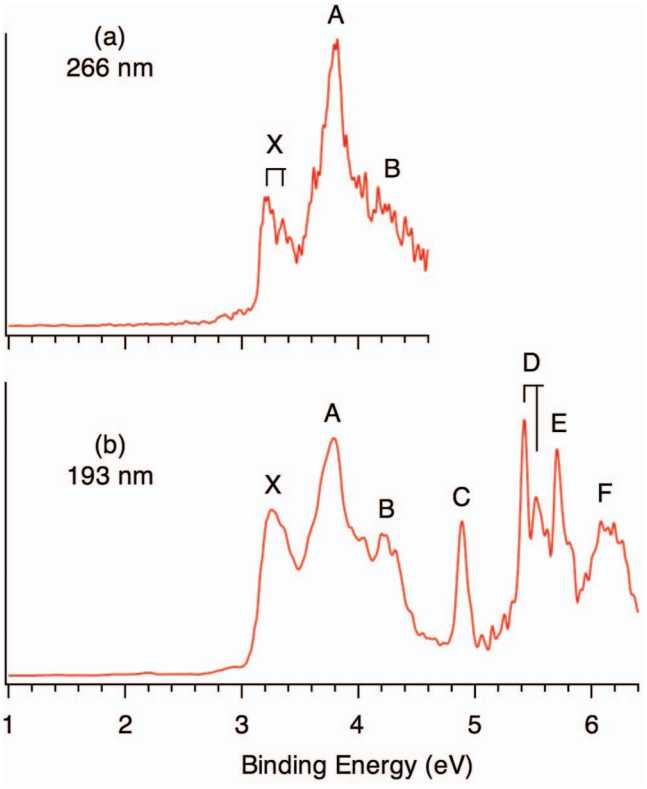

FIG. 2. Photoelectron spectra of $B_3Au_2^-$ at (a) 266 nm and (b) 193 nm. The vertical lines represent resolved vibrational structures.

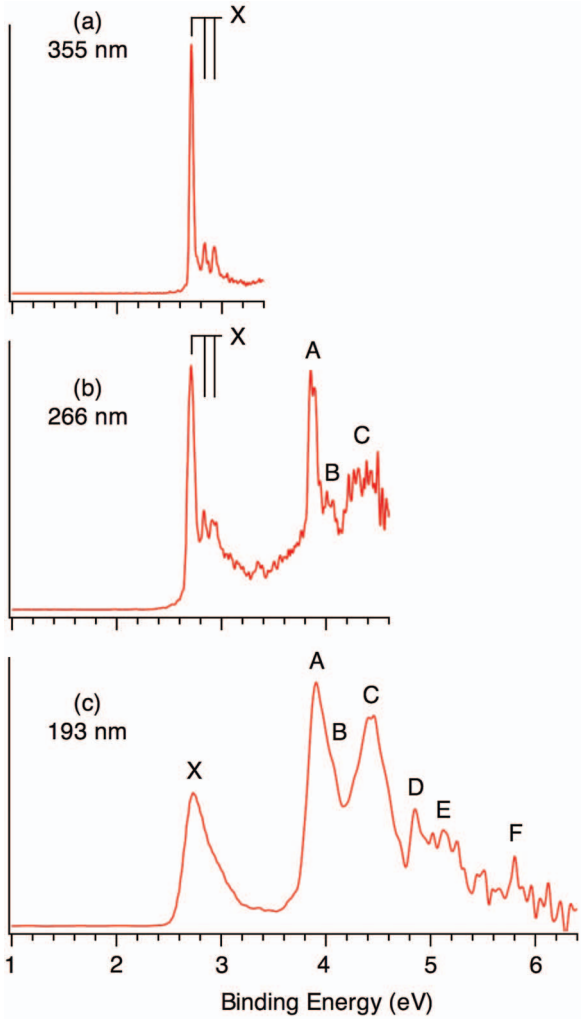

FIG. 3. Photoelectron spectra of B_4O^- at (a) 355 nm, (b) 266 nm, and (c) 193 nm. The vertical lines represent resolved vibrational structures.

unless stated otherwise. All cluster structures presented were obtained initially via the CK structural searches and subsequently optimized at the B3LYP/B,O/aug-cc-pVTZ/Au/Stuttgart_rsc_1997_ecp+2f1g level. Relative energies for the low-lying anion structures within 20 kcal/mol were further refined at the single-point CCSD(T) level.

A. B_3Au^- and B_3Au

Only a handful of structures, **1–5**, are located for the B_3Au^- anion cluster, as shown in Fig. S1 in the supplementary material.[59] The global minimum is **1** (C_{2v}, $^2A_1$) (Fig. 5), in which Au is attached to an apex of the triangular B_3 core. Alternative structures based on a B_3 motif, either triangular or linear, are located ∼17 and ∼25 kcal/mol above the global minimum at the B3LYP level: **2** (C_{2v}, $^2A_1$) and **3** ($C_{\infty v}$, $^2\Sigma$). Structure **2** involves a bridging Au, which is a first-order saddle point and converts to **1** upon optimization, whereas the structure **3** has a terminal Au ligand. At the single-point CCSD(T) level, **2** is ∼7 kcal/mol above **1**. Structures with a B_2 unit, **4** ($C_{\infty v}$, $^2\Sigma$) and **5** (C_{2v}, $^2A_1$), appear at significantly higher energies. The neutral B_3Au structure, **6** (C_{2v}, $^1A_1$), is similar to the corresponding anion global minimum (**1**).

B. $B_3Au_2^-$ and B_3Au_2

The optimized structures for $B_3Au_2^-$ (**7–20**) are shown in Fig. S2 in the supplementary material.[59] The global minimum **7** (C_{2v}, $^1A_1$) (Fig. 5) is built by attaching two Au atoms to two apex sites of the B_3 triangle, which is more stable than the nearest isomer by at least 16 kcal/mol at the B3LYP level. All other structures (**8–20**) are much higher in energy. The neutral B_3Au_2 structure **21** (C_{2v}, $^2B_1$) (Fig. 5) closely resembles the anion global minimum (**7**), except that the quasi-linear ∠BBAu bond angle is more bent by ∼4° in the anion (168°), as compared to 172° in the neutral.

C. B_4O^- and B_4O

We found two closely lying structures for B_4O^-: **22** (C_{2v}, $^2A_1$) and **23** (C_s, $^2A'$) (Fig. 5), which are within ∼1 kcal/mol at both the B3LYP and single-point CCSD(T) levels (Fig. S3)[59] and have similar bond distances with each other. The higher symmetry C_{2v} structure is a first order saddle point with an imaginary frequency of -383 cm^{-1} at the B3LYP level. However, with ZPE corrections included, this structure lies 0.10 kcal/mol lower than the C_s at the B3LYP level, and thus the vibrationally averaged structure of B_4O^- should be C_{2v}. Additional calculations are performed for the C_{2v} structure at the BP86/aug-cc-pVTZ and CCSD/6-311+G(d) levels, both giving a first-order saddle point with an imaginary

This article is copyrighted as indicated in the article. Reuse of AIP content is subject to the terms at: http://scitation.aip.org/termsconditions. Downloaded to IP: 128.148.231.12 On: Mon, 26 May 2014 19:58:53

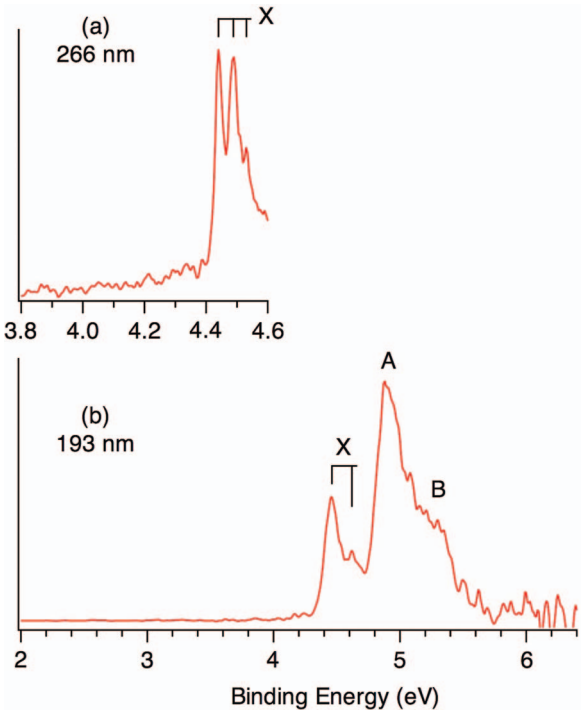

FIG. 4. Photoelectron spectra of $B_5O_2^-$ at (a) 266 nm and (b) 193 nm. The vertical lines represent resolved vibrational.

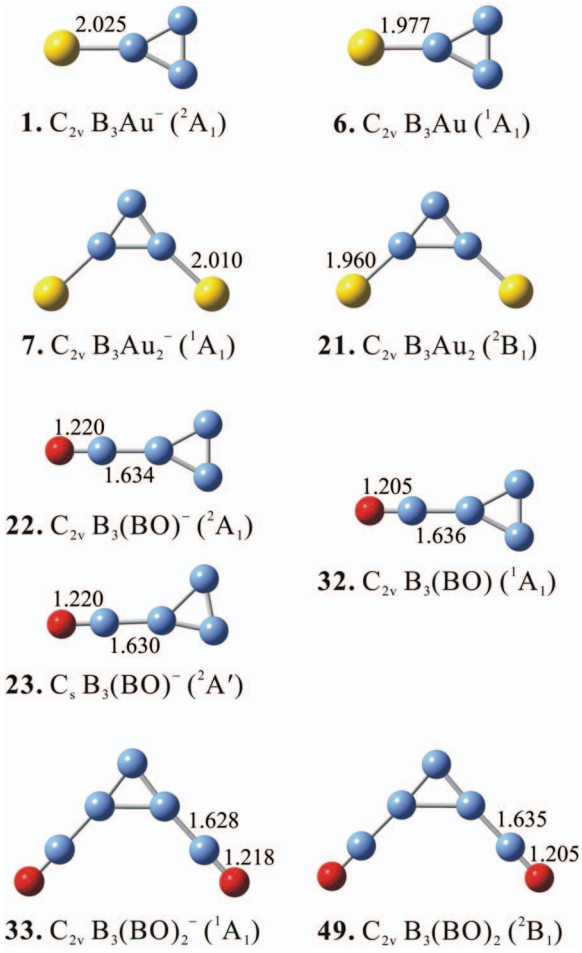

FIG. 5. Optimized structures of $B_3Au_n^-$ and $B_3(BO)_n^-$ (n = 1, 2) clusters and their neutrals at the B3LYP/B,O/aug-cc-pVTZ/Au/Stuttgart_rsc_1997_ecp+2f1g level.

frequency of −285 and −238 cm^{-1}, respectively. With ZPE corrections, the C_{2v} structure is 0.33 and 0.06 kcal/mol more stable than the C_s structure at the BP86 and CCSD levels, respectively. Both structures can be viewed as a BO unit interacting with a B_3 motif, similar to that of B_3Au^-. Alternative structures (**24–31** in Fig. S3)[59] are at least 16 kcal/mol higher in energy.

D. $B_5O_2^-$ and B_5O_2

The global minimum of $B_5O_2^-$, **33** (C_{2v}, $^1A_1$) (Fig. 5), also involves a B_3 core bonded to two BO groups terminally. The closest-lying isomer is a linear cluster, **34** ($D_{\infty h}$, $^1\Sigma_g$), which is higher in energy by ∼11 kcal/mol at B3LYP level (Fig. S4).[59] Other structures (**35–48**; Fig. S4) are at least ∼20 kcal/mol above the global minimum, which contain a B_3, B_4, or B_5 core with terminal BO or bridging O ligands. The neutral structure **49** (C_{2v}, $^2B_1$) (Fig. 5) is similar to the corresponding anion (**33**): the quasi-linear ∠BB(BO) bond angle is slightly less bent by ∼2° in the neutral (176°) than that in the anion (174°). Note again that the global minima of $B_5O_2^-$ and $B_3Au_2^-$ exhibit the Au/BO isolobal analogy, even though they have very different potential energy surfaces.

V. COMPARISON BETWEEN EXPERIMENT AND THEORY

A. B_3Au^- and B_4O^- [$B_3(BO)^-$]

The PES spectra of the B_3Au^- and B_4O^- clusters are remarkably similar, except for a blue shift in binding energies in the latter. This spectral similarity is borne out by their structural similarity, because B_4O^- should be formulated as $B_3(BO)^-$ (**22**, Fig. 5). The calculated ground-state ADEs/VDEs at the B3LYP level are 2.45/2.47 and 2.87/2.89 eV for B_3Au^- **1** (C_{2v}, $^2A_1$) and B_4O^- **22** (C_{2v}, $^2A_1$), respectively (Tables I and II). Compared to the experimental data, the calculated ADEs/VDEs appear to be overestimated by ∼0.2 eV. Note that at all the B3LYP, BP86, and CCSD levels, the B_4O^- **22** (C_{2v}, $^2A_1$) structure is a first-order saddle point on the potential energy surface. The true minimum **23** (C_s, $^2A'$) structure yields the predicted ADE/VDE of 2.90/3.12 eV (Table SI),[59] which deviate substantially from the experimental data by +0.19/+0.41 eV, suggesting that it is unlikely the carrier for the observed PES spectra. This observation can be understood on the ground that the energy difference between **22** (C_{2v}, $^2A_1$) and **23** (C_s, $^2A'$) structures is smaller than their ZPEs. Thus, the B_4O^- cluster is structurally fluxional with respect to an in-plane distortion of the B_3 unit, resulting in the vibrationally averaged structure **22** (C_{2v}, $^2A_1$) as observed.

For the calculated excited electronic states of B_3Au^- and B_4O^-, those from the GKT calculations are in good agreement with experimental data, as shown in Tables I and II. However, the TD-B3LYP results appear to show larger errors for certain detachment channels, failing to reproduce the correct spectral patterns. For instance, the X−A gaps (B_3Au^-: 0.99 eV; B_4O^-: 1.17 eV), which represent the energy gaps between the highest occupied molecular orbitals (HOMOs) and

This article is copyrighted as indicated in the article. Reuse of AIP content is subject to the terms at: http://scitation.aip.org/termsconditions. Downloaded to IP: 128.148.231.12 On: Mon, 26 May 2014 19:58:53

TABLE II. Experimental adiabatic and vertical detachment energies (ADEs and VDEs; in eV) from the photoelectron spectra of B_4O^- and $B_5O_2^-$ clusters, as compared with those calculated using the generalized Koopmans' theorem and the time-dependent B3LYP (TD-B3LYP) methods.

	Expt.		Theor. (GKT)[a]		Theor. (TD-B3LYP)[a]	
Species	Feature	*ADE*/VDE[b,c]	MO[d]	*ADE*/VDE[c,d]	Final state	*ADE*/VDE[c]
B_4O^-	X	*2.71* (2)/2.71 (2)[e]	a_1 (α)	*2.87*/2.89 (S)[f]	$^1A_1$	*2.87*/2.89
	A	3.88 (3)	b_1 (β)	3.90 (T)	$^3B_1$	3.71
	B	4.03 (3)	b_1 (α)	4.00 (S)	$^3A_1$	4.03
	C	4.43 (5)	a_1 (β)	4.41 (T)	$^3B_2$	4.18
	D	4.85 (3)	a_1 (α)	4.70 (S)	$^1B_1$	4.40
	E	~5.2	b_2 (β)	4.98 (T)	$^1A_1$	5.28
	F	5.80 (2)	b_2 (α)	5.79 (S)	$^1B_2$	6.45
$B_5O_2^-$	X	*4.44* (2)/4.44 (2)[e]	b_1 (α)	*4.31*/4.45 (D)[f]	$^2B_1$	*4.31*/4.45
	A	4.90 (5)	a_1 (α)	4.86 (D)	$^2B_1$	4.87
	B	~5.2	b_2 (α)	5.01 (D)	$^2A_2$	5.14

[a]Calculated on the basis of structure **22** (C_{2v}, $^2A_1$), which is a first-order saddle point. Those calculated from the true minimum **23** (C_s, $^2A'$) structure are listed in Table SI in the supplementary material. With the inclusion of the zero-point energy, it is expected that **22** is the vibrationally averaged structure being observed; see text for details.
[b]Numbers in the parentheses represent experimental uncertainties in the last digit.
[c]Shown in *italic* is the ground-state ADE, that is, the electron affinity of the neutral cluster.
[d]Molecular orbital from which the electron is detached. Labels "α" and "β" denote majority and minority spins, respectively; whereas labels "S," "D," and "T" denote singlet, doublet, and triplet final states, respectively.
[e]Observed symmetric ground-state vibrational frequencies for B_4O neutral cluster are 730 ± 50 and 1020 ± 50 cm^{-1}, and those for B_5O_2 neutral cluster are 370 ± 30 and 1280 ± 50 cm^{-1}.
[f]Calculated ground-state *ADE*/VDE at CCSD(T)//B3LYP/aug-cc-pVTZ level are *2.57*/2.55 for B_4O^- and *4.40*/4.53 for $B_5O_2^-$, where the ADE for B_4O^- is artificially larger than VDE due to the fact that the **22** (C_{2v}, $^2A_1$) anion is not a true minimum.

lowest unoccupied molecular orbitals (LUMOs) of the corresponding closed-shell neutrals, are significantly underestimated at the TD-B3LYP level (B_3Au^-: 0.65 eV; B_4O^-: 0.82 eV). Overall, the performance of the GKT method seems to be more consistent and reliable for these open-shell clusters than the TD-B3LYP method.[60,61]

B. $B_3Au_2^-$ and $B_5O_2^-$ [$B_3(BO)_2^-$]

The PES spectra of $B_3Au_2^-$ (Fig. 2) and $B_5O_2^-$ (Fig. 4) are also similar with a very large blue shift in the BO species, which makes the 266 nm spectrum of $B_3Au_2^-$ remarkably similar to the 193 nm of $B_5O_2^-$. This spectral similarity is again reflected by the structural similarity of the two clusters because $B_5O_2^-$ should be formulated as $B_3(BO)_2^-$ (**33**, Fig. 5). The calculated ground state ADEs/VDEs at the B3LYP level are 3.04/3.21 and 4.31/4.45 eV for $B_3Au_2^-$ **7** (C_{2v}, $^1A_1$) and $B_5O_2^-$ **33** (C_{2v}, $^1A_1$), respectively, in excellent agreement with the experimental values of 3.17/3.22 and 4.44/4.44 eV. The calculated VDEs for the excited states of B_3Au_2 and B_5O_2 are also in good agreement with the experiment (Tables I and II). In these cases, the GKT and TD-B3LYP methods seem to perform equally well, probably because of the fact that both anions are closed-shell.

C. Vibrational structure analyses

It is remarkable that vibrational fine structures are observed for the ground state transitions of all four species, as well as for the A and B bands of B_3Au^-, hinting that these anionic clusters and their corresponding neutrals are of relatively high symmetry and little geometric change occurs upon electron detachment. The calculated ground-state vibrational frequencies at the B3LYP level can be used to assign the observed vibrational structures. Notably, the observed ground-state frequencies of 1040 and 1020 cm^{-1} for B_3Au and $B_3(BO)$, respectively, are readily assigned to the B−B stretching of the B_2 unit, calculated as 1089 and 1167 cm^{-1}. The observed modes of ~1150 and 1280 cm^{-1} for B_3Au_2 and $B_3(BO)_2$, respectively, are assigned to the B_3 breathing mode, which are calculated to be 1242 and 1344 cm^{-1}. These assignments are consistent with the nature of the corresponding HOMOs of the anion clusters from which the electron is detached in each case (Fig. 6): σ MOs that are primarily localized on the B_2 unit in B_3Au^- and $B_3(BO)^-$ versus delocalized π MOs over the B_3 motif in $B_3Au_2^-$ and $B_3(BO)_2^-$.

An additional vibrational peak at 2.93 eV for $B_3(BO)$ (Fig. 3) is due to a combination band with a lower mode of 730 cm^{-1} for the B−(BO) stretching, which is predicted to be 513 cm^{-1}. The vibrational structures for excited-state bands A/B of B_3Au, 1170/1200 cm^{-1} (Fig. 1), are assigned to the B_3 breathing, whose predicted value is 1251 cm^{-1} (for the ground state). This assignment is also consistent with the nature of the delocalized π MO (Fig. 6(b)), from which the electron is detached. Lastly, a lower frequency mode (370 cm^{-1}) for the ground-state X of $B_3(BO)_2$ (Fig. 4(a)) is assigned to BO bending (predicted value: 275 cm^{-1}), which is consistent with the slight bond angle change of the quasi-linear ∠BB(BO) angle from the anion to neutral (by ~2°). In summary, the vibrational information provides further support for the identified global-minimum structures for both the anionic and neutral clusters.

VI. DISCUSSION

A. Cluster structures

The good agreement between the experimental and computational results lends considerable credence to the identified

This article is copyrighted as indicated in the article. Reuse of AIP content is subject to the terms at: http://scitation.aip.org/termsconditions. Downloaded to IP: 128.148.231.12 On: Mon, 26 May 2014 19:58:53

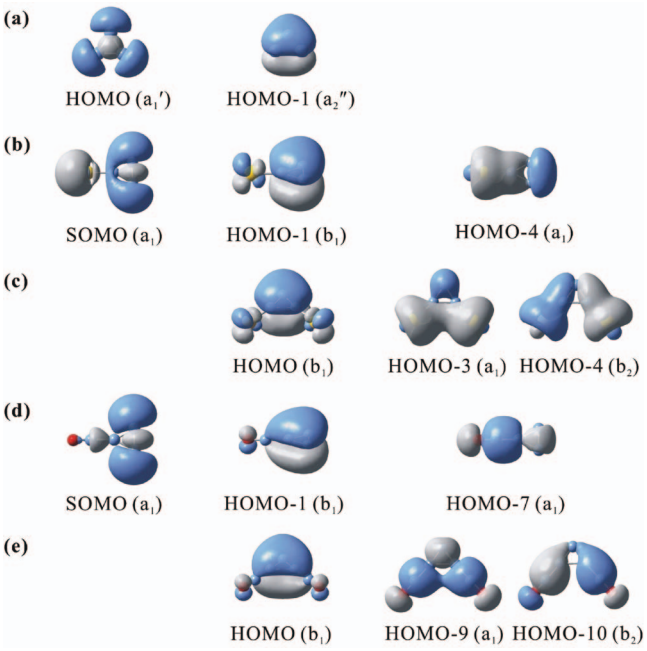

FIG. 6. Selected molecular orbitals of $B_3Au_n^-$ and $B_3(BO)_n^-$ ($n = 1, 2$) that are responsible for the delocalized σ and π bonding in the B_3 core, and the B−Au and B−(BO) σ single bonds.

global-minimum structures for B_3Au^-, $B_3Au_2^-$, B_4O^-, and $B_5O_2^-$, which are similar to those of the B_3H and B_3H_2 clusters.[24,28] The global minima of the B–Au and B–(BO) clusters are all highly stable, with the nearest low-lying structures being higher in energy by as much as ~17, 16, 16, and 11 kcal/mol, respectively, at the B3LYP level (Figs. S1–S4).[59] The results agree well with the experimental observation that there is no hint of any presence of low-lying isomers in the PES spectra. The boron oxide clusters B_4O^- and $B_5O_2^-$, each containing a B_3 core with one or two BO groups, are found to bear no structural relationship to the neat B_4^- and B_5^- clusters, respectively.[6,7] The structures of B_4O^- and $B_5O_2^-$ clusters are completely governed by the BO groups and can be formulated as boron boronyl complexes: $B_3(BO)_n^-$ ($n = 1, 2$), similar to what we have found previously in other B-rich boron oxide clusters.[32–40] This structural feature establishes the isostructural link between $B_3Au^-/B_3Au_2^-$ and $B_4O^-/B_5O_2^-$ and underlies the similarities in their PES spectra. Note that the B–Au, B–(BO), and BO bond distances in $B_3Au_n^-$ and $B_3(BO)_n^-$ ($n = 1, 2$) and their neutrals fall in the ranges of 1.960–2.025, 1.628–1.636, and 1.205–1.220 Å, respectively (Fig. 5), which are typical for the B–Au single bonds, B–(BO) single bonds, and B≡O triple bonds.[13,14,30]

B. Chemical bonding: Aromaticity versus localized core-ligand σ bonds

Key MOs for $B_3Au_n^-$ and $B_3(BO)_n^-$ ($n = 1, 2$) that are responsible for the delocalized bonding within the B_3 core and for the localized 2c–2e σ bonds between the B_3 core and the Au or BO ligands are depicted in Fig. 6, in comparison with those of B_3^-.[6] The full sets of occupied valence MOs for the four clusters are shown in Figs. S5–S9.[59] The bare B_3^- cluster possesses one completely delocalized bonding π MO (HOMO–1) and one completely delocalized bonding σ MO (HOMO) (Fig. 6(a)), rendering it doubly aromatic with 2π and 2σ electrons according to the $(4n + 2)$ Hückel rule. Since both Au and BO are monovalent σ ligands, the delocalized 2σ electrons are used in the $B_3Au_n^-$ and $B_3(BO)_n^-$ ($n = 1, 2$) clusters to form new 2c–2e terminal σ bonds (Figs. 6(b)–6(e)), thus diminishing the σ aromaticity. On the other hand, the π MO retains nearly intact in $B_3Au_n^-$ and $B_3(BO)_n^-$ ($n = 1, 2$), which can be viewed as π aromatic systems in the B_3 core. The nucleus independent chemical shift (NICS)[62] was calculated for the $B_3Au_n^-$ and $B_3(BO)_n^-$ ($n = 1, 2$) clusters and their neutrals at 1.0 Å above the geometric center of the B_3 unit (Table SIV).[59] All NICS values are negative, consistent with π aromaticity. The drop of NICS values for the B_3Au_2 and $B_3(BO)_2$ neutrals is consistent with the fact that only one π electron is present in these systems. An opposite trend is observed for B_3Au^- and $B_3(BO)^-$, for which the anions have smaller NICS values relative to the neutrals. This is probably due to the fact that the neutrals for these two clusters are highly stable electronic systems with large HOMO-LUMO gaps.

C. Beyond the BO/Au analogy: Electron affinity trends of B_3Au_n and $B_3(BO)_n$ ($n = 0–2$)

The similarities between the $B_3Au_n^-$ and $B_3(BO)_n^-$ ($n = 1, 2$) clusters provide new examples for the BO/Au analogy in boron compound clusters, as recently found in $B_{10}Au^-/B_{11}O^-$ and $B_{12}Au^-/B_{13}O^-$.[14,15] However, we note some subtle differences in the trend of EAs as a function of the number of ligands in B_3Au_n and $B_3(BO)_n$ ($n = 1, 2$), which is depicted more clearly in Fig. 7. The slight drop in EA values for B_3Au and $B_3(BO)$ is due to the distortion and destabilization of the σ MOs (Figs. 6(b) and 6(d)) upon the attachment of the first Au/BO ligand. On the other hand, the sizeable increase in EAs for B_3Au_2 and $B_3(BO)_2$ is primarily attributed to the closed-shell electron configurations of the corresponding anions and to the change in nature of the frontier MOs (from σ to π; Fig. 6).

It is known that a B–(BO) cluster possesses a higher EA than its B–Au counterpart. For example, the EAs of $B_{10}(BO)$ and $B_{12}(BO)$ are 0.47 and 0.42 eV higher than those of $B_{10}Au$ and $B_{12}Au$, respectively.[14,15] Similarly, the current $B_3(BO)$ cluster has an EA that is 0.42 eV higher than that of B_3Au. Remarkably, the EA value of $B_3(BO)_2$ is substantially higher than that of B_3Au_2, by as much as 1.27 eV (Fig. 7; Tables I and II). The high EAs for the B–(BO) clusters are due to two effects. First, the partial participation of the BO groups in π conjugation leads to extended delocalization over B_4 (in B_4O) or B_5 (in B_5O_2) (Figs. 6(d) and 6(e)), which helps stabilize the π MOs and the systems as a whole. Second and more importantly, the polar nature of the BO group can induce substantial electrostatic stabilization to the $B_3(BO)_n^-$ ($n = 1, 2$) clusters, resulting in the very large EA for the diboronyl $B_3(BO)_2$ cluster. Both the above effects appear to be accumulative. Thus, multiple boronyl ligands are capable of generating novel species with extremely high EAs,

This article is copyrighted as indicated in the article. Reuse of AIP content is subject to the terms at: http://scitation.aip.org/termsconditions. Downloaded to IP: 128.148.231.12 On: Mon, 26 May 2014 19:58:53

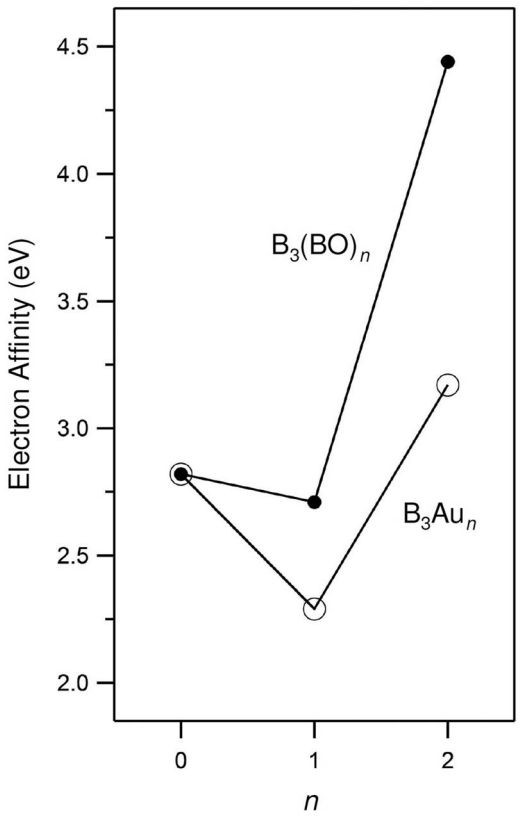

FIG. 7. Evolution of electron affinities of B_3Au_n and $B_3(BO)_n$ ($n = 0–2$) clusters as a function of the number of Au/BO ligands. The electron affinity of B_3 is taken from Ref. 6.

which may warrant further experimental and computational explorations.

VII. CONCLUSIONS

We report a combined photoelectron spectroscopy and density-functional theory study on the structural and electronic properties and chemical bonding in a series of compound clusters between the doubly (π and σ) aromatic B_3 core and the Au or BO ligands: $B_3Au_n^-$ and $B_3(BO)_n^-$ ($n = 1, 2$). These B_3–Au and B_3–(BO) complexes show similar PES patterns with each other, due to the fact that Au and BO are both monovalent σ ligands and the $B_3Au_n^-$ and $B_3(BO)_n^-$ clusters can be considered to be isostructural and isovalent. The B_3 core in the clusters is shown to contain a fully delocalized π orbital, rendering them π aromatic. The combined experimental and theoretical results provide new examples for the Au/BO isolobal analogy and enrich the chemistry of boronyl as a novel inorganic ligand, which are topics of current interest.

ACKNOWLEDGMENTS

This work was supported by the US National Science Foundation (CHE-1263745 to L.-S.W.) and the National Natural Science Foundation of China (Grant No. 21243004 to S.-D.L.).

[1]W. N. Lipscomb, *Boron Hydrides* (Benjamin, New York, 1963); W. N. Lipscomb, Science **196**, 1047 (1977).
[2]C. Präsang, M. Hofmann, G. Geiseler, W. Massa, and A. Berndt, Angew. Chem., Int. Ed. **41**, 1526 (2002); C. Präsang, A. Mlodzianowska, Y. Sahin, M. Hofmann, G. Geiseler, W. Massa, and A. Berndt, *ibid.* **41**, 3380 (2002); W. Mesbah, C. Präsang, M. Hofmann, G. Geiseler, W. Massa, and A. Berndt, *ibid.* **42**, 1717 (2003); For a review, see C. Präsang, A. Mlodzianowska, G. Geiseler, W. Massa, M. Hofmann, and A. Berndt, Pure Appl. Chem. **75**, 1175 (2003).
[3]A. N. Alexandrova, A. I. Boldyrev, H. J. Zhai, and L. S. Wang, Coord. Chem. Rev. **250**, 2811 (2006); D. Yu. Zubarev and A. I. Boldyrev, J. Comput. Chem. **28**, 251 (2007).
[4]I. Boustani, Phys. Rev. B **55**, 16426 (1997); J. E. Fowler and J. M. Ugalde, J. Phys. Chem. A **104**, 397 (2000); J. I. Aihara, H. Kanno, and T. Ishida, J. Am. Chem. Soc. **127**, 13324 (2005).
[5]E. Oger, N. R. M. Crawford, R. Kelting, P. Weis, M. M. Kappes, and R. Ahlrichs, Angew. Chem., Int. Ed. **46**, 8503 (2007).
[6]H. J. Zhai, L. S. Wang, A. N. Alexandrova, A. I. Boldyrev, and V. G. Zakrzewski, J. Phys. Chem. A **107**, 9319 (2003).
[7]H. J. Zhai, L. S. Wang, A. N. Alexandrova, and A. I. Boldyrev, J. Chem. Phys. **117**, 7917 (2002).
[8]H. J. Zhai, A. N. Alexandrova, K. A. Birch, A. I. Boldyrev, and L. S. Wang, Angew. Chem., Int. Ed. **42**, 6004 (2003); H. J. Zhai, B. Kiran, J. Li, and L. S. Wang, Nature Mater. **2**, 827 (2003); B. Kiran, S. Bulusu, H. J. Zhai, S. Yoo, X. C. Zeng, and L. S. Wang, Proc. Natl. Acad. Sci. U.S.A. **102**, 961 (2005); A. P. Sergeeva, D. Yu. Zubarev, H. J. Zhai, A. I. Boldyrev, and L. S. Wang, J. Am. Chem. Soc. **130**, 7244 (2008); W. Huang, A. P. Sergeeva, H. J. Zhai, B. B. Averkiev, L. S. Wang, and A. I. Boldyrev, Nature Chem. **2**, 202 (2010).
[9]A. N. Alexandrova, A. I. Boldyrev, H. J. Zhai, L. S. Wang, E. Steiner, and P. W. Fowler, J. Phys. Chem. A **107**, 1359 (2003); A. N. Alexandrova, A. I. Boldyrev, H. J. Zhai, and L. S. Wang, *ibid.* **108**, 3509 (2004); Z. A. Piazza, W. L. Li, C. Romanescu, A. P. Sergeeva, L. S. Wang, and A. I. Boldyrev, J. Chem. Phys. **136**, 104310 (2012).
[10]A. P. Sergeeva, B. B. Averkiev, H. J. Zhai, A. I. Boldyrev, and L. S. Wang, J. Chem. Phys. **134**, 224304 (2011).
[11]A. P. Sergeeva, Z. A. Piazza, C. Romanescu, W. L. Li, A. I. Boldyrev, and L. S. Wang, J. Am. Chem. Soc. **134**, 18065 (2012).
[12]L. M. Wang, W. Huang, B. B. Averkiev, A. I. Boldyrev, and L. S. Wang, Angew. Chem. Int. Ed. **46**, 4550 (2007); B. B. Averkiev, D. Yu. Zubarev, L. M. Wang, W. Huang, L. S. Wang, and A. I. Boldyrev, J. Am. Chem. Soc. **130**, 9248 (2008); B. B. Averkiev, L. M. Wang, W. Huang, L. S. Wang, and A. I. Boldyrev, Phys. Chem. Chem. Phys. **11**, 9840 (2009).
[13]H. J. Zhai, L. S. Wang, D. Yu. Zubarev, and A. I. Boldyrev, J. Phys. Chem. A **110**, 1689 (2006).
[14]H. J. Zhai, C. Q. Miao, S. D. Li, and L. S. Wang, J. Phys. Chem. A **114**, 12155 (2010).
[15]H. Bai, H. J. Zhai, S. D. Li, and L. S. Wang, Phys. Chem. Chem. Phys. **15**, 9646 (2013).
[16]Q. Chen, H. J. Zhai, S. D. Li, and L. S. Wang, J. Chem. Phys. **138**, 084306 (2013).
[17]A. N. Alexandrova, H. J. Zhai, L. S. Wang, and A. I. Boldyrev, Inorg. Chem. **43**, 3552 (2004); A. N. Alexandrova, A. I. Boldyrev, H. J. Zhai, and L. S. Wang, J. Chem. Phys. **122**, 054313 (2005).
[18]C. Romanescu, A. P. Sergeeva, W. L. Li, A. I. Boldyrev, and L. S. Wang, J. Am. Chem. Soc. **133**, 8646 (2011); T. R. Galeev, C. Romanescu, W. L. Li, L. S. Wang, and A. I. Boldyrev, J. Chem. Phys. **135**, 104301 (2011); W. L. Li, C. Romanescu, T. R. Galeev, L. S. Wang, and A. I. Boldyrev, J. Phys. Chem. A **115**, 10391 (2011).
[19]C. Romanescu, T. R. Galeev, W. L. Li, A. I. Boldyrev, and L. S. Wang, Angew. Chem., Int. Ed. **50**, 9334 (2011); T. R. Galeev, C. Romanescu, W. L. Li, L. S. Wang, and A. I. Boldyrev, *ibid.* **51**, 2101 (2012); W. L. Li, C. Romanescu, T. R. Galeev, Z. Piazza, A. I. Boldyrev, and L. S. Wang, J. Am. Chem. Soc. **134**, 165 (2012).
[20]D. Z. Li, Q. Chen, Y. B. Wu, H. G. Lu, and S. D. Li, Phys. Chem. Chem. Phys. **14**, 14769 (2012); W. L. Li, C. Romanescu, T. Jian, and L. S. Wang, J. Am. Chem. Soc. **134**, 13228 (2012).
[21]M. Sironi, M. Raimondi, D. L. Cooper, and J. Gerratt, J. Phys. Chem. **95**, 10617 (1991).
[22]J. K. Olson and A. I. Boldyrev, Comput. Theor. Chem. **967**, 1 (2011).
[23]C. W. Yoon, P. J. Carroll, and L. G. Sneddon, J. Am. Chem. Soc. **131**, 855 (2009).
[24]R. Hernandez and J. Simons, J. Chem. Phys. **96**, 8251 (1992).
[25]N. Gonzales and J. Simons, J. Chem. Phys. **101**, 10746 (1994).

This article is copyrighted as indicated in the article. Reuse of AIP content is subject to the terms at: http://scitation.aip.org/termsconditions. Downloaded to IP: 128.148.231.12 On: Mon, 26 May 2014 19:58:53

[26]J. Moc, Eur. Phys. J. D **45**, 247 (2007).
[27]E. Earl, R. Hernandez, and J. Simons, J. Chem. Phys. **97**, 8357 (1992).
[28]E. Miliordos and A. Mavridis, J. Chem. Phys. **132**, 164307 (2010).
[29]T. B. Tai and M. T. Nguyen, Chem. Phys. Lett. **483**, 35 (2009).
[30]H. J. Zhai, L. M. Wang, S. D. Li, and L. S. Wang, J. Phys. Chem. A **111**, 1030 (2007).
[31]H. J. Zhai, S. D. Li, and L. S. Wang, J. Am. Chem. Soc. **129**, 9254 (2007).
[32]S. D. Li, H. J. Zhai, and L. S. Wang, J. Am. Chem. Soc. **130**, 2573 (2008).
[33]W. Z. Yao, J. C. Guo, H. G. Lu, and S. D. Li, J. Phys. Chem. A **113**, 2561 (2009).
[34]H. J. Zhai, J. C. Guo, S. D. Li, and L. S. Wang, ChemPhysChem **12**, 2549 (2011).
[35]Q. Chen, H. J. Zhai, S. D. Li, and L. S. Wang, J. Chem. Phys. **137**, 044307 (2012).
[36]D. Z. Li, H. Bai, Q. Chen, H. G. Lu, H. J. Zhai, and S. D. Li, J. Chem. Phys. **138**, 244304 (2013).
[37]D. Yu. Zubarev, A. I. Boldyrev, J. Li, H. J. Zhai, and L. S. Wang, J. Phys. Chem. A **111**, 1648 (2007).
[38]S. D. Li, J. C. Guo, and G. M. Ren, J. Mol. Struct.: THEOCHEM **821**,153 (2007).
[39]C. Q. Miao and S. D. Li, Sci. China Chem. **54**, 756 (2011).
[40]C. Q. Miao, H. G. Lu, and S. D. Li, J. Cluster Sci. **24**, 233 (2013).
[41]M. L. Drummond, V. Meunier, and B. G. Sumpter, J. Phys. Chem. A **111**, 6539 (2007); M. T. Nguyen, M. H. Matus, V. T. Ngan, D. J. Grant, and D. A. Dixon, *ibid.* **113**, 4895 (2009); C. B. Shao, L. Jin, L. J. Fu, and Y. H. Ding, Mol. Phys. **107**, 2395 (2009).
[42]E. D. Jemmis, G. Subramanian, and G. N. Srinivas, J. Am. Chem. Soc. **114**, 7939 (1992).
[43]A. A. Korkin, P. v. R. Schleyer, and M. L. McKee, Inorg. Chem. **34**, 961 (1995).
[44]J. K. Olson and A. I. Boldyrev, Inorg. Chem. **48**, 10060 (2009).
[45]B. Kiran, X. Li, H. J. Zhai, L. F. Cui, and L. S. Wang, Angew. Chem., Int. Ed. **43**, 2125 (2004).
[46]X. Li, B. Kiran, and L. S. Wang, J. Phys. Chem. A **109**, 4366 (2005).
[47]B. Kiran, X. Li, H. J. Zhai, and L. S. Wang, J. Chem. Phys. **125**, 133204 (2006).
[48]D. Yu. Zubarev, J. Li, L. S. Wang, and A. I. Boldyrev, Inorg. Chem. **45**, 5269 (2006).
[49]L. S. Wang, H. S. Cheng, and J. Fan, J. Chem. Phys. **102**, 9480 (1995).
[50]J. Akola, M. Manninen, H. Hakkinen, U. Landman, X. Li, and L. S. Wang, Phys. Rev. B **60**, R11297 (1999); L. S. Wang and X. Li, in *Clusters and Nanostructure Interfaces*, edited P. Jena, S. N. Khanna, and B. K. Rao (World Scientific, New Jersey, 2000), pp. 293–300.
[51]M. Saunders, J. Comput. Chem. **25**, 621 (2004); P. P. Bera, K. W. Sattelmeyer, M. Saunders, and P. v. R. Schleyer, J. Phys. Chem. A **110**, 4287 (2006).
[52]J. P. Perdew, K. Burke, and M. Ernzerhof, Phys. Rev. Lett. **77**, 3865 (1996).
[53]P. J. Hay and W. R. Wadt, J. Chem. Phys. **82**, 299 (1985).
[54]T. H. Dunning, J. Chem. Phys. **90**, 1007 (1989); R. A. Kendall, T. H. Dunning, and R. J. Harrison, *ibid.* **96**, 6796 (1992); K. L. Schuchardt, B. T. Didier, T. Elsethagen, L. Sun, V. Gurumoorthi, J. Chase, J. Li, and T. L. Windus, J. Chem. Inf. Model. **47**, 1045 (2007); J. M. L. Martin and A. Sundermann, J. Chem. Phys. **114**, 3408 (2001).
[55]D. J. Tozer and N. C. Handy, J. Chem. Phys. **109**, 10180 (1998).
[56]M. E. Casida, C. Jamorski, K. C. Casida, and D. R. Salahub, J. Chem. Phys. **108**, 4439 (1998); R. Bauernschmitt and R. Ahlrichs, Chem. Phys. Lett. **256**, 454 (1996).
[57]J. Cizek, Adv. Chem. Phys. **14**, 35 (1969); G. E. Scuseria and H. F. Schaefer, J. Chem. Phys. **90**, 3700 (1989); R. J. Bartlett and M. Musial, Rev. Mod. Phys. **79**, 291 (2007).
[58]M. J. Frisch, G. W. Trucks, H. B. Schlegel *et al.*, GAUSSIAN 09, revision A.2, Gaussian, Inc., Wallingford, CT, 2009.
[59]See supplementary material at http://dx.doi.org/10.1063/1.4816010 for the calculated ADEs and VDEs using the generalized Koopmans' theorem (GKT) and time-dependent B3LYP (TD-B3LYP) methods based on structure **23** (C_s, $^2A'$) of B_4O^- (Table SI); theoretical ADEs and VDEs of B_3Au^- and B_4O^- using the time-dependent SVWN5 (TD-SVWN5) and time-dependent PBEPBE (TD-PBEPBE) methods, as compared to those at the TD-B3LYP level (Tables SII and SIII); calculated NICS values at 1.0 Å above the geometric center of the B_3 unit for $B_3Au_n^-/B_3Au_n$ and $B_3(BO)_n^-/B_3(BO)_n$ ($n = 1, 2$) clusters (Table SIV); alternative optimized structures for B_3Au^-, $B_3Au_2^-$, B_4O^-, and $B_5O_2^-$ at the B3LYP level (Figs. S1−S4); and occupied valence molecular orbitals of B_3Au^- **1** (C_{2v}, $^2A_1$), $B_3Au_2^-$ **7** (C_{2v}, $^1A_1$), $B_3(BO)^-$ **22** (C_{2v}, $^2A_1$), $B_3(BO)^-$ **23** (C_s, $^2A'$), and $B_3(BO)_2^-$ **33** (C_{2v}, $^1A_1$) (Figs. S5−S9).
[60]O. A. Vydrov and G. E. Scuseria, J. Chem. Phys. **121**, 8187 (2004).
[61]This statement is true for the cases of B_3Au^- and B_4O^-, yet it remains to be tested for other open-shell species. One reviewer commented that the failure of TD-B3LYP here is likely due to self-interaction errors (SIE) of DFT. This appears not to be entirely true. Our additional calculations using the TD-SVWN5 and TD-PBEPBE methods[60] also fail to reproduce the correct PES patterns for B_3Au^- and B_4O^-; see Tables SII and SIII in the supplementary material[59] for details. The performance of TD-SVWN5 is obviously worse than TD-B3LYP, whereas the TD-PBEPBE data are comparable to those of TD-B3LYP. In summary, all three time-dependent DFT (TD-DFT) methods perform poorly relative to the GKT, despite the fact that the GKT method is a rather crude approximation.
[62]P. v. R. Schleyer, C. Maerker, A. Dransfeld, H. Jiao, and N. J. R. E. Hommes, J. Am. Chem. Soc. **118**, 6317 (1996).

This article is copyrighted as indicated in the article. Reuse of AIP content is subject to the terms at: http://scitation.aip.org/termsconditions. Downloaded to IP: 128.148.231.12 On: Mon, 26 May 2014 19:58:53